Tensile and shear behavior of recycled AA 6060 aluminium chips by direct hot extrusion

Thomas Corre, Jason Perrin, Johannes Gebhard, Théo Duchateau, Lola Lilensten, Mathilde Laurent-Brocq, A. Erman Tekkaya, Bertrand Huneau

Tensile and shear behavior of recycled AA 6060 aluminium chips by direct hot extrusion

Thomas Corre[1], Jason Perrin[1],Johannes Gebhard[4], Théo Duchateau[2,3], Lola Lilensten[3], Mathilde Laurent-Brocq[2], A. Erman Tekkaya[4], Bertrand Huneau[1]

Abstract

Solid state recycling of aluminium chips is a promising technique to reduce environmental impacts of secondary production. As the recycling process induces a highly oriented microstructure, this study aims to quantify the mechanical properties of extrudates and identify the role of chip boundaries in the fracture behavior. Tensile and shear tests are performed on heat treated AA 6060 alloy and analyzed using digital image correlation. The tensile behavior of the chip-based material is similar to its cast-based counterpart, reaching a yield strength of 230 MPa. Shear properties are close for small deformations, although the chip-based material have lower ductility due to the early onset of damage at the chip boundary. These results confirm the industrial relevance of this process for large scale recycling of aluminium.

Keywords

solid state recycling, shear test, chip boundaries, damage mechanisms, aluminium alloys

Introduction

The production of primary aluminium requires substantial amounts of energy and generates a lot of greenhouse gases: up to 200 GJ of primary energy and around 12 t of CO_2 per metric ton of aluminium (Raabe et al. 2022). With a total of 70 Mt/year, the world production of primary aluminium is thus responsible of approximately 2 % of the global CO_2 emissions (37 Gt in 2022 (IEA 2022)). The recycling of aluminium by melting can lead to reductions in energy consumption and CO_2 emissions as high as 95 %, in comparison with the production of primary aluminium (Das et al. 2010). The environmental impact of secondary production can be further mitigated by using solid-state recycling, which requires even less energy. Among the possible processes, the recycling of machined aluminium chips by hot extrusion is an interesting option (Duflou et al. 2015; Gronostajski et al. 2000). In this process, the chips are used without melting and are welded directly during the extrusion thanks to the severe plastic deformation applied. Several processes are developped to directly recycle machined aluminium chips, such as direct rolling (El Mehtedi et al. 2023) or friction stir consolidation (Puleo et al. 2023). Among them, the direct recycling by hot extrusion is an interesting option (Duflou et al. 2015; Gronostajski et al. 2000).

This process has been studied by a few research groups over the years (Tekkaya et al. 2009; Sarkar et al. 2023). Some of these studies investigated the mechanical tensile behavior of chip-based materials obtained by hot extrusion (Güley et al. 2013; Kolpak et al. 2019; Rady et al. 2020; Schulze et al. 2022). For example, Schulze et al. (2022) observed a reduction of only 10 % both in yield strength (YS) and ultimate tensile strength (UTS) for chip-based AA-6060, in comparison to its cast-based counterpart. Fracture surfaces exhibiting chip interfaces are reported in the literature (Güley et al. 2013). The oxide layer at the chip interface has a major role on the quality on the welding between chips (Cooper and Allwood 2014). The surface expansion induced by the hot extrusion process is believed to break this ozxide layer ensuring proper welding of the chips (Kolpak et al. 2019). Recently, a detailed analysis of this oxide layer has been presented by (Laurent-Brocq et al. 2023) with various characterization techniques.

In previous works, the material was only subjected to mechanical loads along the direction of extrusion, either monotonic (Güley et al. 2013; Kolpak et al. 2019; Schulze et al. 2022) or cyclic (Koch et al. 2019). However, during their service life, mechanical parts are subjected to complex multiaxial loading. It is therefore important to characterize the chip-based material behavior under different solicitations, such as shear. In this case, the chip boundaries may be unfavourably oriented with respect to the stress state and are thus expected to play a greater role. Moreover, the aluminium extrudates were generally tested without any post-process precipitation hardening heat treatment.

The objective of the present paper is thus to investigate the mechanical resistance of heat treated chip-based extrudates,

[1] Nantes Université, Ecole Centrale Nantes, CNRS, GeM, UMR 6183, F-44000 Nantes, France
[2] Univ. Paris Est Creteil, CNRS, ICMPE, UMR 7182, 2 rue Henri Dunant, 94320 Thiais, France
[3] Chimie ParisTech, PSL Research University, CNRS, Institut de Recherche de Chimie Paris,75005 Paris, France
[4] Institute of Forming Technology and Lightweight Components, TU Dortmund University, 44227 Dortmund, Germany

Corresponding author:
Thomas Corre
Email: thomas.corre@ec-nantes.fr

especially at chip interfaces, for two mechanical solicitation: tension and shear.

Materials and methods

Material production

This study focuses on two materials: an AA-6060 aluminium alloy either processed by extrusion from a cast billet or by direct hot extrusion of cold compacted chips obtained from the same cast billet. The chemical composition of the alloy is given in Table 1. These two materials are designated in the following as cast-based and chip-based, respectively. The chip-based material simulates direct recycling of production scrap, but to ensure comparability of the results, the chips are dry machined by turning from a cast billet for the purpose of this study. The chips have a half torus shape with a total width of 7.7 mm and a thickness of approximately 1.5 mm.

Table 1. Chemical composition of the aluminium alloy.

Element	Al	Si	Mg	Fe	Cu
mass %	bal.	0.435	0.364	0.213	0.028

The chips are then compacted to billets with a diameter of 60 mm, a length of 90 mm and a relative density of 71 %. The cast billets have a diameter of 60 mm and a length of 175 mm and where compacted with a maximum force of 1000 kN. Before extrusion, a high temperature treatment is applied to the billets, both cast-based and chip-based (550^{o}C for 45 min, no gas or vacuum shielding). The hot extrusion experiments are conducted on a 2.5 MN extrusion press heated at 450^{o}C with a container diameter of 66 mm. he bearing length of the die is 6 mm. In each extrusion cycle, either two chip-based billets or one cast billet is extruded with a flat-faced die. The diameter of the extruded round profile is 12 mm, leading to an extrusion ratio of 30.25. The remaining material from a previous cycle and the interface to the new billet, the so-called charge weld, are cut out of the profile. After extrusion, the relative density of both profiles is close to 100 % (Schulze et al. 2022). The process and the chips production is described in further details by Schulze et al. (2022). These extrusion conditions lead to a rather poor welding case: the low extrusion ratio and the round geometry are not favourable to good chip welding (Kolpak et al. 2019). More precisely, the weld quality factor, as defined by Kolpak et al. (2019), is of only 75% at the center of the center of the extrudates (see Appendix). Thus, the aim is to observe the influence of chips in a poorly welded case, and the results of the mechanical tests will be conservative compared to what can be expected on parts with larger extrusion ratios.

Figure 1(a,b) shows the microstructure of the chip-based material at the center of the extruded bars. The chip boundaries, as revealed by etching, are clearly visible. The process strongly elongates the chips and leads to their alignment in the direction of extrusion. The size of these chips is in the order of 100 to 500 micrometers in the direction perpendicular to the extrusion, but they can reach several millimetres along the length of the profile.

A precipitation hardening heat treatment is applied on the material after extrusion, aiming at T6 state. The bars are

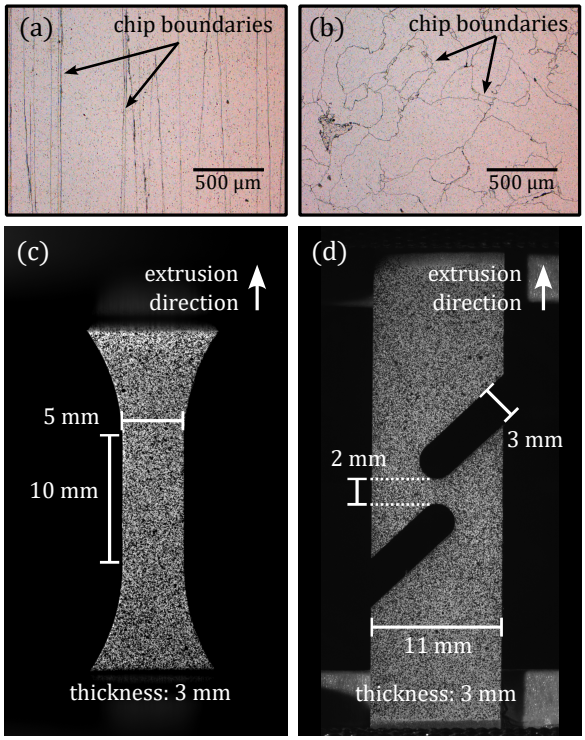

Figure 1. Microstructure of the chip-based extrudates at the center of the profile, in the extrusion direction (a) and transversally (b). Specimen geometries for tensile (c) and shear (d) tests. Note that the speckle pattern is painted.

subjected to a solution heat treatment of 1 h at 550°C, then immediately quenched in water at room temperature. They are then left for 7 days at room temperature for natural aging, and finally undergo artificial aging at 185°C for 8h (Develay 1986; Martinsen et al. 2012; Poznak et al. 2018). The heat treatment induces some localized blistering on the surface of the chip based extrudates. However, this surface effect does not impact material characterization as the specimen are cut out from the center of the profiles. After the heat treatment, the Vickers hardness of the cast-based and chip-based material are 99.8 $\pm$ 2.82 HV and 97.0 $\pm$ 0.82 HV, respectively (applied load: 2.5 kg).

Material characterization

Tensile and shear specimens are machined in the profiles along the extrusion direction. Figure 1(c,d) provides their respective geometries. In particular, the ligament of the shear specimen i.e., the remaining length between the two grooves, is 2 mm long. The gauge zone of each sample is reduced (3×5 mm^2 for tensile and 2×3 mm^2 for shear) and located at the centre of the profile. This ensures a homogeneous microstructure with several chips of similar size across the gauge zone. The weld quality factor in the cross section of each sample is between 75% and 80% (see Appendix). Three samples of each type are made for each material.

The mechanical tests are performed on a universal tensile machine under quasi-static conditions (the imposed displacement is 0.6 mm/min for the tensile tests and 0.5 mm/min for the shear tests). They are monitored with a camera (AVT Prosilica GT 6600) and a black and white speckle pattern is sprayed on the samples to measure the

displacement field by digital image correlations (DIC). Figure 1(c,d) provides examples of the images obtained. For the tensile tests, the strain is obtained from the displacement field with an optical gauge of 10 mm. For shear tests, DIC is used to measure a loading parameter independent of the initial distance between the jaws. By convention, the imposed displacement is approximated here by the difference of the displacement measured at the top and bottom of the specimen, in a zone with no plastic deformation (average over a line at 12.5 mm from the center). The physical size of the pixel is about 20 μm.

The shear tests are also monitored with a second camera to get a close-up of the useful zone in order to measure the deformation field with a better spacial resolution. This camera, placed on the other side of the sample, is mounted with a bi-telecentric lens (magnification $\times$ 4) offering a field of view of 9×6 mm^2. The physical size of the pixel in this case is of approximately 1.4 μm. The images are analyzed using the open-source software Ufreckels (Réthoré 2018), following the global digital image correlation approach (Besnard et al. 2006).

A JEOL 6360 scanning electron microscope (SEM) is finally used for the fracture surfaces analysis. The acceleration voltage is 20 kV and the secondary electrons are used for the imagery.

Results and discussion

Tensile behavior along the extrusion direction

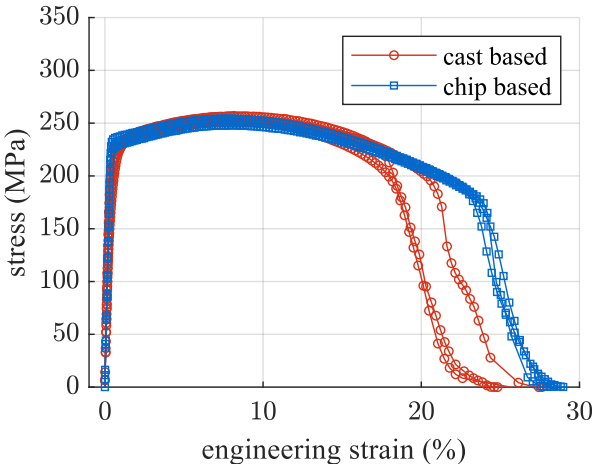

Figure 2. Tensile curves for heat treated chip-based and cast-based materials.

Table 2. Measured tensile properties.

	YS (MPa)	UTS (MPa)
cast-based	235 $\pm$ 2.3	259 $\pm$ 1.0
chip-based	229 $\pm$ 11.6	251 $\pm$ 8.0

The tensile curve for the two materials is shown in Figure 2 and Table 2 provides the averaged values of the yield strength and the ultimate tensile strength. In the direction of extrusion, these properties are very similar: even if these properties are slightly smaller for the chip-based material, of about 3% for both YS and UTS, the observed differences are close to measurement uncertainties. Concerning ductility, the elongation at break is noticeably lower for the cast-based material.

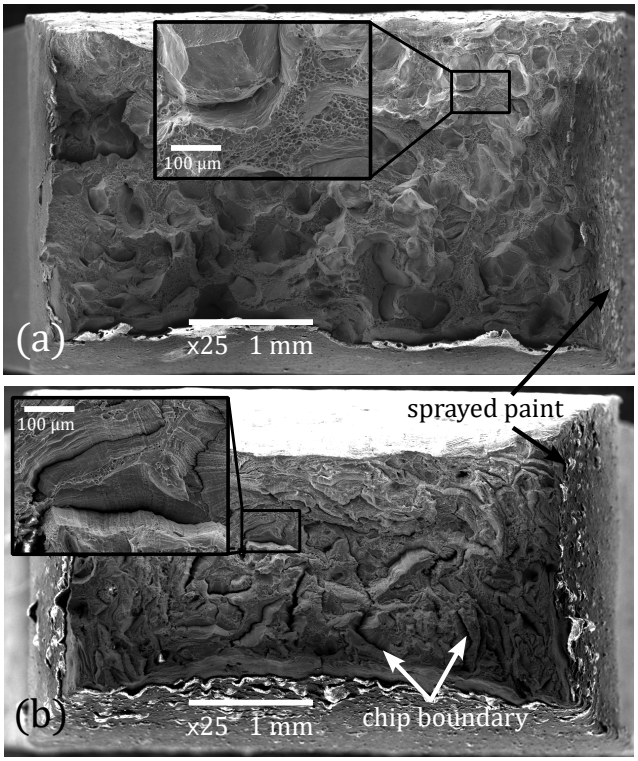

Figure 3. Typical fracture surfaces of the cast-based (a) and chip-based (b) tensile specimens.

The fracture surfaces shown in Figure 3 underline very different damage mechanisms. For the cast-based material, the failure mode shown in Figure 3(a) is both transgranular ductile with dimples, as expected for an aluminum alloy at room temperature, and intergranular ductile (see Fig.3(a) inset), which is less common. However, several authors have already reported this type of fracture surfaces for aluminum alloys with a mixed mode failure (Pardoen et al. 2003), especially in Al-Mg-Si alloys (Prince and Martin 1979).

The fracture surface of the chip-based material (Fig.3(b)) clearly shows the chips, as if they were individually fractured. The shape and size of the delamination zones correspond to the cross-section of the chips in the undeformed extrudates (Fig.1(b)). Two fracture mechanisms are thus observed: a delamination along the chip boundaries and the ductile failure of each chip, indicated by the dimples observed in the middle of the chips. The inset of Fig.3(b) details one of these chips. These observation are consistent with the fracture surfaces reported by Güley et al. (2013).

The tensile mechanical properties (YS and UTS) of the chip-based and cast-based material are very similar despite different fracture mechanisms. The observed gap is even smaller than the 10% difference reported by Schulze et al. (2022) for as-extruded profiles. It then further confirms the practical interest of the process, here associated with a precipitation hardening heat treatment. Indeed, the high values of YS and UTS observed for the chip-based material

are much higher than those reported in the literature (Güley et al. 2013; Kolpak et al. 2019; Schulze et al. 2022). The load curves are also very similar up to 15% strain, but the strain at break is lower for the cast-based material. This observation concerning the strain at break is unexpected. For the cast-based samples, the presence of intergranular fracture, which is known to induce a loss of ductility, might explain this result.

Shear behavior

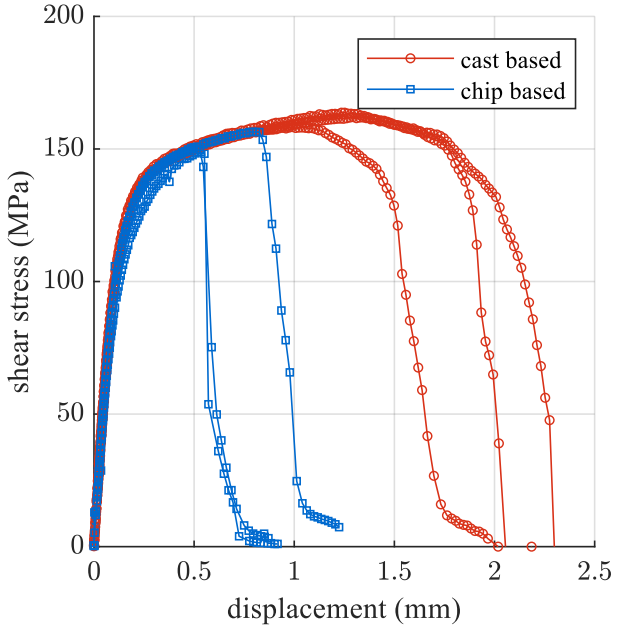

Figure 4. Shear test load curve. The shear stress is the load divided by the ligament surface. The displacement is measured by DIC on a 25 mm gage length centered around the ligament. Each marker corresponds to a picture.

The shear test was chosen to magnify the difference in mechanical behavior between the two materials. As the chip boundaries are mostly aligned with the extrusion direction (Fig.1(a)), they are directly subjected to shear stress in their plane.

Figure 4 shows the global response of the two materials for the shear test. The imposed displacement is measured by DIC (see section 2.2) and the shear stress is computed following the conventional way for shear test (using ASTM B831-93 for instance) i.e., as the load divided by the smallest section of the ligament. Both materials exhibit a very similar response at the beginning of the test, from the elastic to the early elastoplastic deformation. However, a brutal failure is observed for the chip-based material while the cast-based material sustains large plastic deformation. The brutal failure denotes here the quick drop of the load (accompanied by an audible click). Failure of the chip-based material occurs at a smaller imposed displacement i.e., at a lower shear strain, than the cast-based one. As the two materials follow the same load curve before failure, the maximum shear stress reached is only 6 % lower on average for the chip-based material. Figure 5(a,b) shows close-ups of the ligament after failure. The large plastic deformations reached by the cast-based material are clearly visible from the deformed shape of the ligament. By comparison, the sharp crack observed for the chip-based material confirms the brittle fracture mode. The fracture surfaces corresponding to these two side views are reported on the Fig.5(c,d). For the cast-based material, the fracture is severely crushed, but some dimples advocate, if needed, for the ductile failure. On the contrary, the fracture surface of the chip-based material is surprisingly smooth, suggesting that the fracture occurs exactly along the chip boundaries. The texture of the fracture surface supports the hypothesis: the thin lines on the surface (oriented in the extrusion direction) are also visible on the chip boundary delamination in the inset of Fig.3(b). In addition, the fracture surface is not completely flat in the transverse direction but rather follows the uneven shape of the chips.

The chip boundary acts as a weak plane in the material, resulting in an early failure of the chip-based material. As underlined by (Schulze et al. 2022), this type of fracture is similar to failure at the bond in solid-state welded aluminium (Cooper and Allwood 2014). Fig.5(d) shows in our case that the failure plane is composed of multiple welded chip-interfaces in the thickness of the sample. The present shear test is then directly probing the mechanical behavior of the chip boundaries. The next section focuses on the DIC analysis of this damage during the shear test.

Failure of the shear samples

DIC analysis can provide some insight on the specific fracture mechanisms of the chip-based material. The DIC analysis is performed on the close-up pictures of the zone of interest with 16 pixels triangular elements, leading to a spatial resolution of the strain field of approximately 22,4 μm. The detailed analysis for one of the chip-based specimens is shown in Figure 6. Fig.6(a) recalls the load curve of the test (from Fig.4) where each symbol marks a picture analysed with DIC. The black symbols indicates the pictures chosen to illustrate the main features observed. In particular, Fig.6(b) shows the strain field for the last image before failure of the specimen (image 95). Note that the maximum shear strain (or shear parameter) is drawn on the reference configuration. This strain field is not homogeneous and the deformation seems to be localized in bands along the direction of extrusion.

To highlight this heterogeneity, the mean value of the maximum shear strain is computed along the extrusion direction. This is done at different distances from the center of the sample and on 75% of the ligament length to exclude free edge effects (thus over the zone between the white lines in Fig.6(b)). The results are displayed for different load levels in Fig6(c) corresponding to the pictures highlighted in Fig6(a). The localized bands are clearly visible before the fracture, at least for an imposed displacement superior to 0.3 mm (image 80). The bands are 200 μm to 500 μm apart, which is very similar to chip size observed on Fig.1(a). The appearance of these bands is illustrated by the three snapshots Fig.6(d-f) although it is difficult to define a precise threshold at which the phenomenon starts.

The macroscopic crack, responsible for the final failure of the sample, is located at the position of the maximum of the curve for images 95 and 96: it clearly follows one specific deformation band (see also in Fig.6(f)). It is to note that the magnitude of the shear strain measured after failure (i.e. after

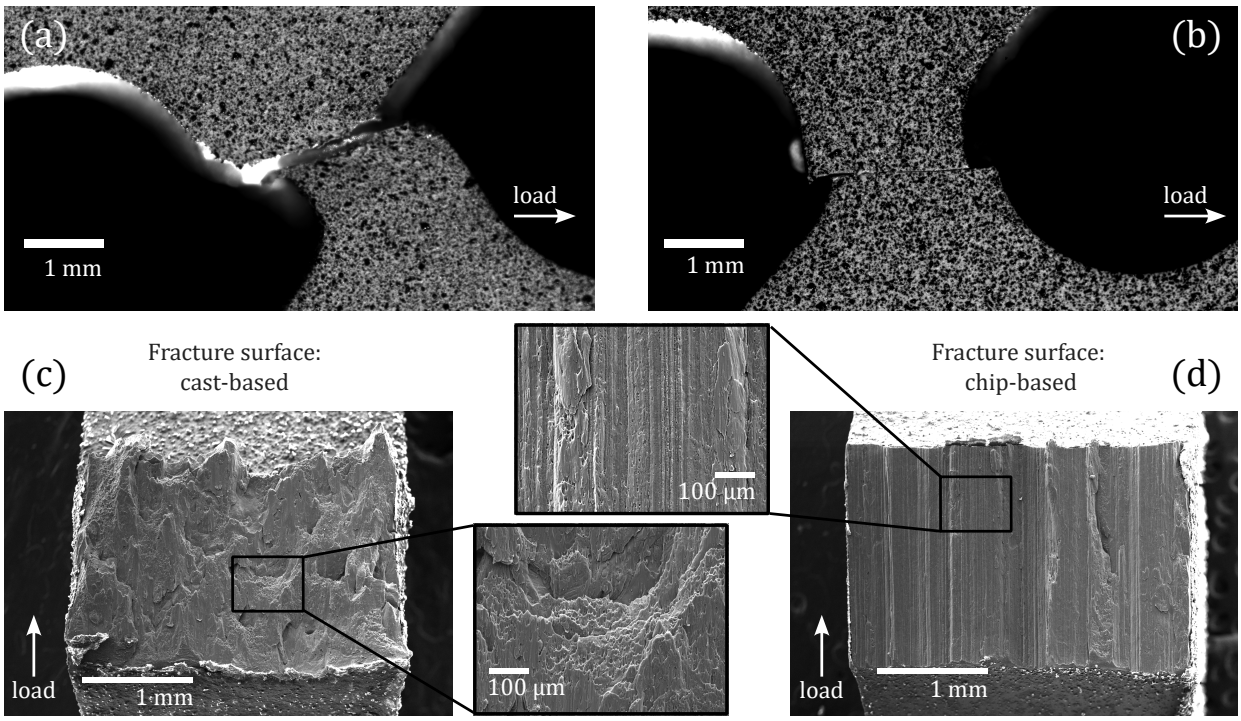

Figure 5. Fracture of the cast-based (a) and chip-based (b) shear specimen. SEM micrographs of the corresponding fracture surfaces (cast-based (c) and chip-based (d)). Magnification: $\times 30$ and $\times 200$.

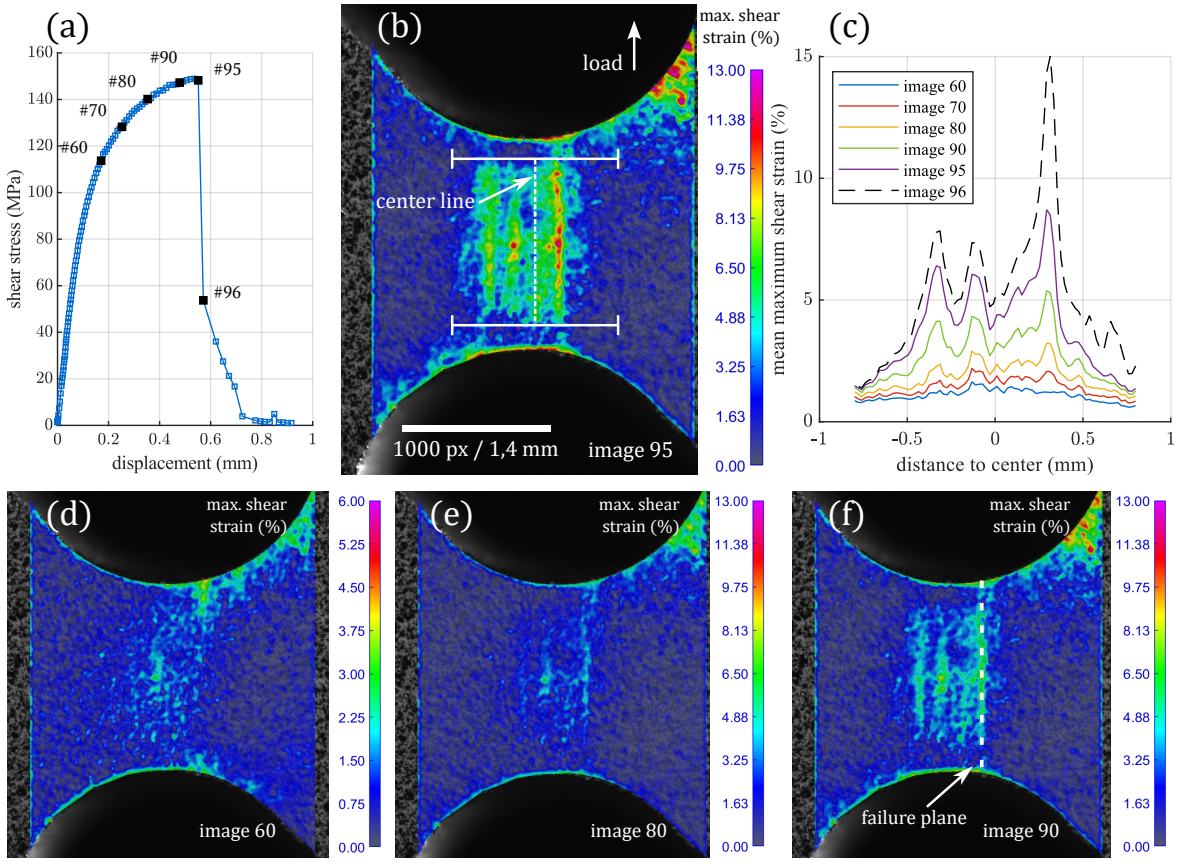

Figure 6. Load curve of a chip-based shear test with the image chosen to illustrate the strain field (a). Maximum shear strain measured from DIC on the last image before fracture, drawn on the undeformed configuration (b). Mean values of the max shear strain computed along the load direction at the centre of the specimen (between the dark lines) (c), for different load level. Maximum shear strain field for three load level (d - f). Note that the scale on snapshot is different (d).

image 95) is irrelevant as a sharp discontinuity crosses the specimen surface (see image in Fig.5(b)). That is why the strain field for image 96 is not shown in Fig.6 and Fig.6(c) features a dotted line.

The spacing of the bands, their orientation and the observation that one of them leads to fracture of the sample strongly suggest they are linked with some damage mechanism at the chip boundary. Indeed, the shear localization can be attributed to a local loss of stiffness, possibly due to crack or void formation inside the material. With this hypothesis, multiple chip boundaries are damaged during loading, before failure occurs on the weakest point. The precise nature of the damage mechanism should be further described but it can be linked to the fracture surfaces observed in tension Fig.3(b).

The number of chip boundaries involved in the damage mechanism remains difficult to assess from surface measurements. In addition, it hinders the specific mechanical characterization of a single interface. From an experimental point of view, Cooper and Allwood (2014) measured a bond shear strength of a solid-state welded aluminium with a model experiment where only one bonding is involved. Moreover, accurate analysis of shear test based on DIC have been proposed in the literature, for example by Reyne et al. (2021), to extract local shear stress to quantify work-hardening, but without damage. These two approaches, that could be used to identify a shear strength for the chip boundaries are unfortunately not directly applicable here, because of the heterogeneity of the damage over the zone of interest and in the thickness. Further investigations are thus needed to be able to isolate the behavior of the chip boundary.

Conclusion

This study presents a mechanical characterization of heat treated chip-based aluminium extrudates under tensile and shear loading. The mechanical tensile properties of the chip-based material are very close to its cast-based counterpart. YS and UTS values of around 230 MPa and 250 MPa respectively, correspond to what is expected for industrial applications. Such high values of YS and UTS are reported for the first time for chip based extrudates of AA 6060-T6.

As expected from the microstructure, the differences of behavior are magnified for loading out of the extrusion direction i.e., off the deformed chip axis. In this way, shear tests along the chip boundary are performed. The beginning of the load curve is similar for both material but the chip based material fails early in a brutal manner. Micrographs show that final fracture occurs along a plane that joins multiple chip interfaces. Full field measurements also suggest that some damage mechanism come into play at multiple chip boundaries before the main crack becomes observable.

However, in spite of the loss of ductility, the maximum shear stresses reached by the two materials are close. This result is promising since the shear ductility is much less critical for extruded parts than for other aluminium processes (sheet forming for instance). In addition, the extrusion condition in this study are sub-optimal and lead to a low chip welding quality. The reported results are thus conservatives. With a view to optimum industrial use, further investigation is needed to establish a precise link between the extrusion conditions and mechanical properties at the chip boundary. To this end, monitored shear tests and the failure mechanisms they highlight appear to be a valuable tool to characterise the mechanical performances of chip-based extrudates.

Appendix: weld quality factor

The weld quality of the extruded profiles was calculated with the modified Kolpak et al. (2019) weld model of Cooper and Allwood (2014). The necessary data were determined with a numerical simulation of the process with an Eulerian approach, using the modified visco-plastic Zener and Hollomon material model (Sellars and Tegart 1972). The used software was Altair Inspire Extrude. The weld quality is determined along the radius of the cross-section of the extruded profile (see Figure 7(a)). Especially in the centre of the profile, the weld quality factor is relatively low at 0.75 but increases towards the outer radius to 0.999 (see Fig.7(b)). Kolpak et al. (2019) stated that a weld quality above 0.95 indicates a successful process without surface delamination.

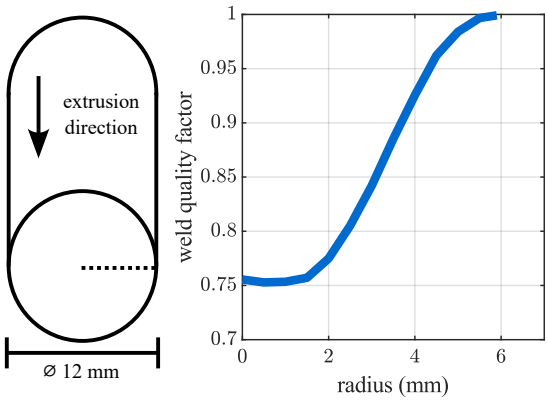

Figure 7. Sketch of the 12 mm extrudate in which the samples are taken. The weld quality factor is numerically calculated along the radius.

Acknowledgement

The authors are grateful to Oliver Schulz for the computation of the weld quality factor.

References

Besnard G, Hild F and Roux S (2006) "Finite-Element" Displacement Fields Analysis from Digital Images: Application to Portevin–Le Châtelier Bands. *Experimental Mechanics* 46(6): 789–803. DOI:10.1007/s11340-006-9824-8.

Cooper DR and Allwood JM (2014) The influence of deformation conditions in solid-state aluminium welding processes on the resulting weld strength. *Journal of Materials Processing Technology* 214(11): 2576–2592.

Das SK, Green JA, Kaufman JG, Emadi D and Mahfoud M (2010) Aluminum recycling—an integrated, industrywide approach. *JOM* 62: 23–26.

Develay R (1986) Traitements thermiques des alliages d'aluminium DOI:10.51257/a-v1-m1290.

Duflou JR, Tekkaya AE, Haase M, Welo T, Vanmeensel K, Kellens K, Dewulf W and Paraskevas D (2015) Environmental assessment of solid state recycling routes for aluminium alloys: Can solid state processes significantly reduce the

environmental impact of aluminium recycling? *CIRP Annals* 64(1): 37–40. DOI:10.1016/j.cirp.2015.04.051.

El Mehtedi M,Buonadonna P, Carta M, El Mohtadi R, Mele A, and Morea D(2023) Sustainability Study of a New Solid-State Aluminum Chips Recycling Process: A Life Cycle Assessment Approach *Sustainability* 15(14), 11434 DOI: 10.3390/su151411434.

Gronostajski J, Marciniak H and Matuszak A (2000) New methods of aluminium and aluminium-alloy chips recycling. *Journal of Materials Processing Technology* 106(1): 34–39. DOI: 10.1016/S0924-0136(00)00634-8.

Güley V, Güzel A, Jäger A, Ben Khalifa N, Tekkaya AE and Misiolek WZ (2013) Effect of die design on the welding quality during solid state recycling of AA6060 chips by hot extrusion. *Materials Science and Engineering: A* 574: 163–175. DOI: 10.1016/j.msea.2013.03.010.

IEA (2022) Co2 emissions in 2022. IEA Paris, France.

Koch A, Wittke P and Walther F (2019) Computed tomography-based characterization of the fatigue behavior and damage development of extruded profiles made from recycled aw6060 aluminum chips. *Materials* 12(15): 2372.

Kolpak F, Schulze A, Dahnke C and Tekkaya AE (2019) Predicting weld-quality in direct hot extrusion of aluminium chips. *Journal of Materials Processing Technology* 274: 116294. DOI:10.1016/j.jmatprotec.2019.116294.

Laurent-Brocq M, Lilensten L, Pinot C, Schulze A, Duchaussoy A, Bourgon J, Leroy E and Tekkaya AE (2023) Solid state recycling of aluminium chips: Multi-technique characterization and analysis of oxidation. *Materialia* 31: 101864. DOI: 10.1016/j.mtla.2023.101864.

Martinsen FA, Ehlers FJH, Torsæter M and Holmestad R (2012) Reversal of the negative natural aging effect in Al–Mg–Si alloys. *Acta Materialia* 60(17): 6091–6101. DOI:10.1016/j.actamat.2012.07.047.

Pardoen T, Dumont D, Deschamps A and Brechet Y (2003) Grain boundary versus transgranular ductile failure. *Journal of the Mechanics and Physics of Solids* 51(4): 637–665. DOI:10.1016/S0022-5096(02)00102-3.

Poznak A, Thole V and Sanders P (2018) The natural aging effect on hardenability in al-mg-si: A complex interaction between composition and heat treatment parameters. *Metals* 8(5): 309.

Prince K and Martin J (1979) The effects of dispersoids upon the micromechanisms of crack propagation in al-mg-si alloys. *Acta Metallurgica* 27(8): 1401–1408.

Puleo R, Latif A, Ingarao G, Di Lorenzo R and Fratini L (2020) Solid bonding criteria design for aluminum chips recycling through Friction Stir Consolidation. *Journal of Materials Processing Technology* 319, 118080 DOI:10.1016/j.jmatprotec.2023.118080

Raabe D, Ponge D, Uggowitzer PJ, Roscher M, Paolantonio M, Liu C, Antrekowitsch H, Kozeschnik E, Seidmann D, Gault B, De Geuser F, Deschamps A, Hutchinson C, Liu C, Li Z, Prangnell P, Robson J, Shanthraj P, Vakili S, Sinclair C, Bourgeois L and Pogatscher S (2022) Making sustainable aluminum by recycling scrap: The science of "dirty" alloys. *Progress in Materials Science* 128: 100947. DOI:10.1016/j.pmatsci.2022.100947.

Rady MH, Mustapa MS, Wagiman A, Al-Alimi S, Shamsudin S, Lajis MA, Mansor MN and Harimon MA (2020) Effect of the heat treatment on mechanical and physical properties of direct recycled aluminium alloy (aa6061). *International Journal of Integrated Engineering* 12(3): 82–89.

Reyne B, Hérault D, Thuillier S and Manach PY (2021) Quality of the strain state in simple shear testing using field measurement techniques. *International Journal of Mechanical Sciences* 208: 106660. DOI:10.1016/j.ijmecsci.2021.106660.

Réthoré J (2018) Ufreckles. DOI:10.5281/zenodo.1433776. URL https://doi.org/10.5281/zenodo.1433776.

Sarkar A, Razavi N, Ringen G and Welo T (2023) Assessing the fatigue behaviour of recycled Al-alloys: A critical review. *Materialia* 32: 101938. DOI:10.1016/j.mtla.2023.101938.

Schulze A, Hering O and Tekkaya AE (2022) Production and Subsequent Forming of Chip-Based Aluminium Sheets Without Remelting. *International Journal of Precision Engineering and Manufacturing-Green Technology* 9(4): 1035–1048. DOI:10.1007/s40684-021-00395-8.

Sellars C and Tegart WM (1972) Hot workability. *International Metallurgical Reviews* 17(1): 1–24.

Tekkaya AE, Schikorra M, Becker D, Biermann D, Hammer N and Pantke K (2009) Hot profile extrusion of AA-6060 aluminum chips. *Journal of Materials Processing Technology* 209(7): 3343–3350. DOI:10.1016/j.jmatprotec.2008.07.047.